JACS
JOURNAL OF THE AMERICAN CHEMICAL SOCIETY
pubs.acs.org/JACS
Article

Molecular Design of Chemically Fueled Peptide–Polyelectrolyte Coacervate-Based Assemblies

Fabian Späth, Carsten Donau, Alexander M. Bergmann, Moritz Kränzlein, Christopher V. Synatschke, Bernhard Rieger, and Job Boekhoven*

Cite This: J. Am. Chem. Soc. 2021, 143, 4782–4789
Read Online
ACCESS | Metrics & More | Article Recommendations | Supporting Information

ABSTRACT: Complex coacervated-based assemblies form when two oppositely charged polyelectrolytes combine to phase separate into a supramolecular architecture. These architectures range from complex coacervate droplets, spherical and worm-like micelles, to vesicles. These assemblies are widely applied, for example, in the food industry, and as underwater or medical adhesives, but they can also serve as a great model for biological assemblies. Indeed, biology relies on complex coacervation to form so-called membraneless organelles, dynamic and transient droplets formed by the coacervation of nucleic acids and proteins. To regulate their function, membraneless organelles are dynamically maintained by chemical reaction cycles, including phosphorylation and dephosphorylation, but exact mechanisms remain elusive. Recently, some model systems also regulated by chemical reaction cycles have been introduced, but how to design such systems and how molecular design affects their properties is unclear. In this work, we test a series of cationic peptides for their chemically fueled coacervation, and we test how their design can affect the dynamics of assembly and disassembly of the emerging structures. We combine them with both homo- and block copolymers and study the morphologies of the assemblies, including morphological transitions that are driven by the chemical reaction cycle. We deduce heuristic design rules that can be applied to other chemically regulated systems. These rules will help develop membraneless organelle model systems and lead to exciting new applications of complex coacervate-based examples like temporary adhesives.

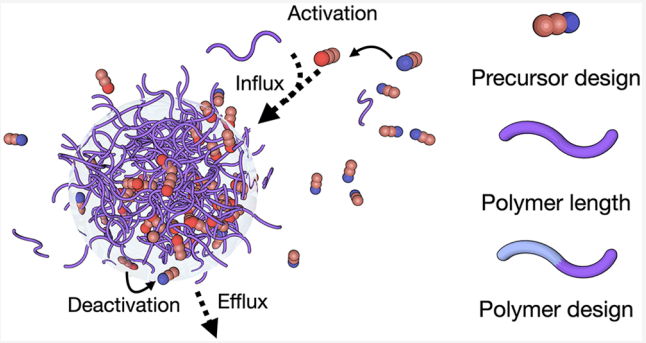

Downloaded via TU MUENCHEN on April 3, 2021 at 19:48:09 (UTC).
See https://pubs.acs.org/sharingguidelines for options on how to legitimately share published articles.

INTRODUCTION

Complex coacervate-based assemblies comprise two oppositely charged polyelectrolytes that phase separate to form a polyelectrolyte-rich phase in a polyelectrolyte-dilute solution.[1] The assemblies formed by complex coacervation range from droplets, complex coacervate core micelles that can be spherical or worm-like micelles, to polymersomes,[2−4] and find application in the food, pharmaceutical, and personal care industries.[5−9] Nature also uses emerging properties when two polyelectrolytes are brought together, such as underwater adhesives used by marine organisms like the sandcastle worm.[10,11] In these adhesive sites, coacervate-based assemblies are formed by two oppositely charged proteins and represent a dynamic and transient phase that facilitates adhesion, but the exact details are often unclear.[12] Another prominent natural assembly formed by the complexation of polyelectrolytes is the class of membraneless organelles. These droplet-like organelles, which are ubiquitous in eukaryotic cells, e.g., nucleoli, Cajal bodies, P-bodies, or stress granules, rely on the phase separation of RNA and proteins to form liquid compartments.[13] Interestingly, most of these droplets are highly dynamic and transient, i.e., they only temporarily exist and perform their function before redissolving.[14−16] It was recently discovered that their transient nature and their dynamic properties are regulated by nonequilibrium reactions that consume ATP as they progress.[17] Thus, membraneless organelles can be active droplets, i.e., droplets whose properties are regulated by energy-driven chemical reactions, and their transient and dynamic nature can also be regulated by chemical reactions.[18,19] However, many of the underlying biological mechanisms that regulate these droplet-based organelles remain elusive.

Experimental model systems for biological complex coacervate-based assemblies can answer open questions related to complex coacervation in biology. Initial studies focused on complex coacervate-based droplets that exist close to equilibrium,[1,4,20] and later work studied droplets that are

Received: January 29, 2021
Published: March 22, 2021

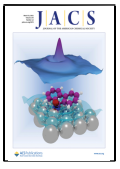

ACS Publications
© 2021 American Chemical Society

regulated by nonequilibrium chemical reactions. For example, it was shown that the phase-separation of RNA could be chemically regulated by enzymatic phosphorylation or dephosphorylation of a cationic peptide.[21]

Our group recently introduced a synthetic complex coacervate system that is regulated by an energy-consuming chemical reaction cycle.[22] A zwitterionic peptide is converted into a cationic one in a carbodiimide-consuming activation reaction. In essence, the activation reaction converts an aspartate-based C-terminus into its corresponding acid anhydride (Scheme 1A). This activation increases the affinity

Scheme 1. Schematic Representation of the Design of Active Coacervate-Based Droplets[a]

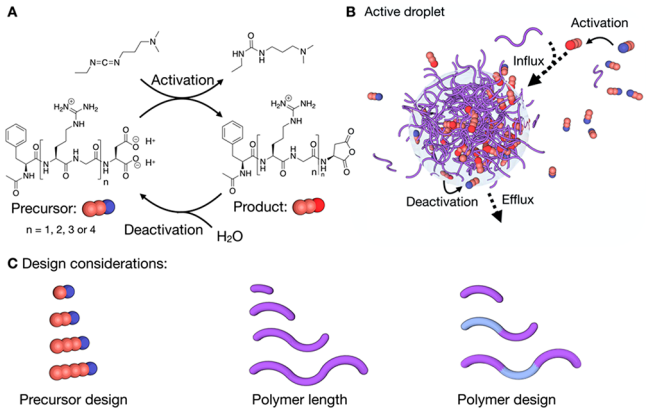

[a](A) Chemical reaction cycle that transiently activates peptides for coacervation. (B) Schematic representation of an active coacervate-based droplet. Upon activation of the precursor (blue), the product can bind an anionic polymer (purple strands). Strands with activated peptides are held together through complex coacervation to form a droplet. Simultaneously, the activated product is reverted to precursor through deactivation, which leads to the expulsion of the peptide from the droplet.

to anionic polymers, and when a sufficient amount of peptide is activated, the increased affinity can lead to coacervate-based droplet formation. Simultaneously, hydrolysis of the anhydride reverts the activation, which undoes its affinity for RNA. The result is a dynamic interplay between droplet material flowing into the droplets by activation and droplet material leaving the droplet through deactivation (Scheme 1B). As such, this system is an excellent model for biological counterparts of coacervate-based active assemblies like membraneless organelles and marine adhesive, particularly when the role of chemical reactions and how these regulate droplet properties are studied. However, we currently lack clear design rules for coacervate-based active assemblies. Moreover, we also do not know which parameters affect the dynamics of assembly and disassembly of these assemblies. Tailoring the building blocks of our dissipative complex coacervates is necessary to further elucidate their dynamic properties in response to our proposed reaction cycle. Therefore, in this work, we introduce rules on how the dynamics of our active droplets can be regulated through molecular design. We test the effect of the peptide design on the dynamics of the emerging droplets, as well as the effect of the polymer length. Finally, we introduce a polymer design that changes the morphology of our complex coacervation-based assemblies (Scheme 1C).

RESULTS AND DISCUSSION

Role of Peptide Design. In the first part of this study, we focus on how the peptide design affects droplets' emergence and dynamics. We varied the number of RG-repeats in our peptide design to tune the electrostatic interactions between our peptides and the anionic polymers (Figure 1A). At the lowest extreme (peptide **1**), our peptide consisted of one RG-repeat. At the other extreme (peptide **4**), our peptide comprised four RG-repeats. Given that C-terminal aspartic acid has a −2 charge, the overall charge of the precursor state of the peptides is −1, 0, +1, +2, respectively (Figure 1B). These peptides were synthesized using solid-phase peptide synthesis (see Supporting Information). We tested for the formation of droplets for each of our four peptides in response to chemical fuel. We used a plate reader to measure the absorbance at 600 nm as a measure for turbidity, and we used confocal microscopy with sulforhodamine as a fluorescent dye to examine the nature of the turbidity. For all experiments, we used a concentration of 16 mM peptide in 200 mM MES buffer at pH 5.3. As an anionic polymer, we used polystyrenesulfonate (PSS) of 17 kg/mol. The concentration of the PSS was 25 mM, expressed as styrenesulfonate monomer units. We tested for the emergence of turbidity by the addition of 50 mM of EDC as fuel.

For peptide **1**, no increased turbidity was observed, and confocal microscopy confirmed the absence of assemblies (Figure 1C,D). Peptide **1** does also not form droplets with longer PSS strands up to 1000 kg/mol after up to 200 mM of EDC were added (Figure S12 A). In contrast, the addition of fuel to peptide **2** resulted in the formation of droplets evidenced by confocal microscopy (Figure 1C). The emergence and decay of droplets was completed within 15 min. We found that the solution's turbidity rapidly evolved, i.e., it rapidly increased, peaked at around 2 min, after which it decayed rapidly to its original level (Figure 1D). The fast rates and high dynamics reflect the fast kinetics of our reaction cycle on which we will comment in the next paragraph. Lower amounts of EDC shorten the lifetime, whereas higher amounts of EDC lead to prolonged turbidity (e.g., 21 min for 100 mM of EDC, Figure S6). Different peptide-to-EDC ratios also lead to different lifetimes since the amount of EDC that is available per precursor is changed, too (Figure S7). For the next peptide, peptide **3**, a similar response was observed. However, the decay in the turbidity was delayed compared to peptide **2**. Specifically, it took almost 20 min for the original transparent solution to recover. In contrast, peptide **4** formed coacervate droplets before the addition of fuel (see Figure 1C). The addition of fuel did not alter the turbidity or the nature of the droplets (Figure 1D, Figure S13). The turbidity of this sample did decrease over the course of the experiments. However, even after 1 h, it was still present, and the droplets started sedimenting. Peptide **4** also did not form dynamic coacervates with other PSS lengths (Figure S12 B). All samples were also refueled with 50 mM of EDC, which led to a reproducible transient increase of turbidity in solutions containing peptides **2** and **3** indicating that the system can be recycled (Figure S14). Finally, we introduce peptide **3-NH$_2$** (Ac-F(RG)$_3$N-NH$_2$, Figure 1A), which is similar to **3**, except for that we substituted the C-terminal aspartic acid for the amidated asparagine C-terminus. This mutation makes **3-NH$_2$** permanently cationic 3+. Indeed, **3-NH$_2$** formed droplets at a

https://doi.org/10.1021/jacs.1c01148
J. Am. Chem. Soc. 2021, 143, 4782−4789

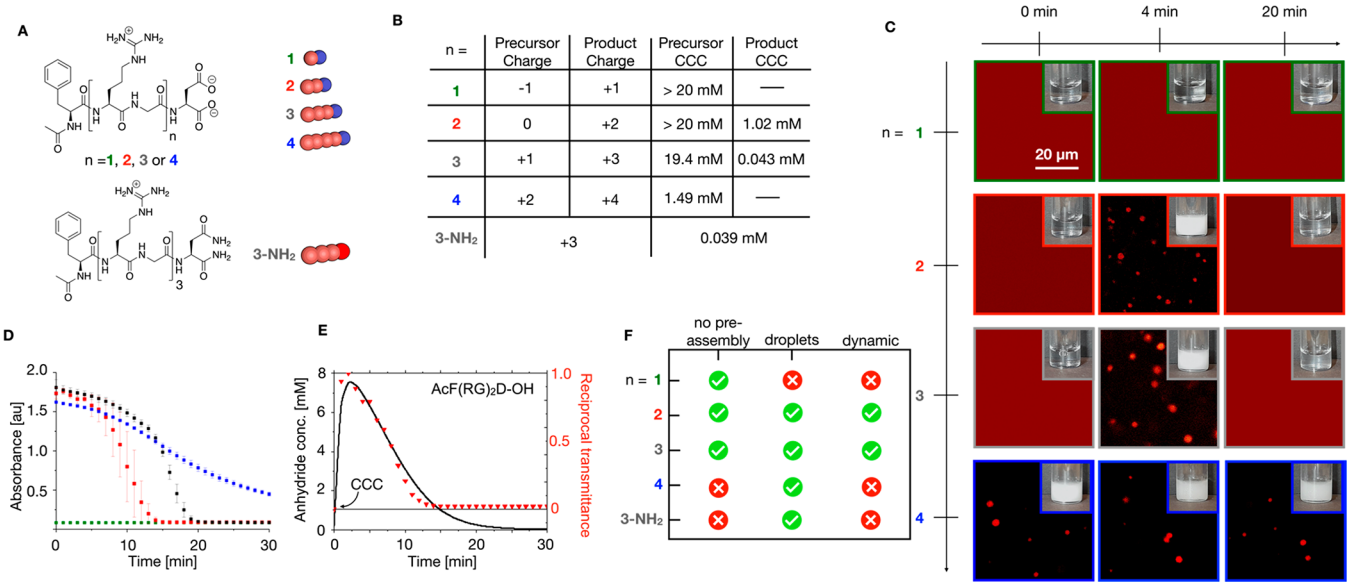

Figure 1. Effect of molecular design of the peptide on droplet behavior. (A) Molecular structures of the peptide sequences used in this study. (B–F) Response of the system when 16 mM peptide is fueled with 50 mM EDC in the presence of 25 mM PSS (17 kg/mol) expressed in monomer units and 200 mM MES buffer at pH 5.3: (B) CCC values and changes in charges of the different peptide structures after activation with EDC and conversion into the anhydride. A nonactive model peptide (**3-NH$_2$**) was also tested to compare it to the active peptides. (C) Confocal laser scanning microscopy micrographs acquired at various time-points during the reaction cycle. The insets show photographs of the sample at the same time-points. The scale bar represents 20 μm. (D) Absorbance at 600 nm as a function of time as measured with a plate reader. (E) Overlay of the anhydride concentration of peptide **2** (left axis) and the reciprocal transmittance (right axis) as a function of time. The overlap of the traces demonstrates the high degree of correlation between the chemical reaction cycle and the presence of droplets. The concentration profile is predicted by the kinetic model. The CCC is drawn as a black line at 1.02 mM. The reciprocal transmittance is calculated by $10^{(\text{Absorbance})}$ and then normalized to 1. We plotted the maximum normalized reciprocal transmittance such that the *x*-axis corresponds to the CCC on the left *y*-axis. (F) Summary of the different responses of the systems with the different peptides **1**–**4** and **3-NH$_2$**.

concentration above 0.039 mM (Figure 1B). As such, **3-NH$_2$** is a great model compound for the active state of **3**.

To better understand the dynamic evolution of the droplets, we tested the kinetics of the reaction cycle under conditions described above by analytical HPLC in combination with a previously developed quench method,[23] and a kinetic model (see Supporting Information). For each peptide, the concentrations of EDC, the peptide, and its corresponding product were monitored in response to 50 mM EDC. As expected, the decay of the EDC and the emergence and decay of the product evolved very similarly for peptides **1**, **2**, and **3**. That means, for all peptides, all EDC was consumed in 15 min, whereas the peptide's corresponding product emerged, peaked at around 2 min, and was deactivated after roughly 18 min. The evolution of the reaction cycle could be predicted accurately with our kinetic model. Interestingly, for peptides **1**, **2**, and **3**, the same rate constants were used for each reaction to obtain good fits (Figure S15), which suggests that the chemical reactivity for each peptide is the same and is independent of the presence or absence of droplets, given that **1** never forms droplets, but **2** and **3** do. The evolution of the reaction cycle with peptide **4** was not measured in the presence of PSS, because the turbid solutions were too viscous to be injected in the HPLC.

We correlated the evolution of the turbidity to the evolution of the kinetics of the reaction cycle to better understand how peptide design affects droplet dynamics. We first converted the turbidity to reciprocal transmittance, which, unlike turbidity, scales linearly with increasing total droplet volume (see Supporting Information). We assess the droplets' dynamics by comparing three events in the reaction cycle: (1) the time points where the anhydride concentration and the reciprocal transmittance reach their maximum, (2) half of their maximum value, and (3) the time where the reciprocal transmittance reaches its original value compared to when the concentration anhydride reaches the concentration required for coacervation. We first measured this critical concentration required for coacervation (CCC, critical coacervation concentration) to be 1.02 mM for the product of **2** and 0.043 mM for the product of **3** (see Supporting Information). Noteworthy, the CCC for the anhydride of peptide **3** is a close match to the CCC of model compound **3-NH$_2$**. The CCC of **3** and **4** without EDC was 1.49 and 19.4 mM, respectively (Figure 1B).

The evolution of the reciprocal transmittance of peptide **2** in response to EDC correlated strongly with the evolution of the kinetics of the reaction cycle; i.e., both maxima were reached after 3 min, the droplets disappeared when the concentration anhydride fell below the CCC after 15 min, and half of the maximums were obtained after 8.5 and 7.5 min, respectively (Figure 1E). The evolution of the turbidity of peptide **3** also correlated with the evolution of the kinetics of the reaction cycles, albeit less strongly. Half of the maximum of turbidity was reached after 11 min, while the peptide anhydride concentration showed a half-life time of 9 min (Figure S16), indicating a minimal delay from the maximum until complete dissolution as soon as the CCC is reached after 20 min. Unsurprisingly, the correlations of peptides **1** and **4** that formed no droplets or permanent droplets, respectively, were poor (Figure S16).

We classify the response of our system to chemical fuel in four categories, i.e., (i) no droplets emerge; the droplets that emerge are (ii) dynamic or (iii) metastable; and droplets are

https://doi.org/10.1021/jacs.1c01148
J. Am. Chem. Soc. 2021, 143, 4782–4789

present before the addition of fuel (iv) (Figure 1F). In this classification, dynamic means that droplets follow the behavior of the reaction cycle with a high correlation. In other words, in dynamic droplets, the kinetics of the reaction cycle are regulating the properties of the droplets. This strong correlation is evident for peptides **2** and **3**. For these peptides, droplets form as soon as the CCC for the peptide anhydride is reached. This threshold is exceeded almost instantly after EDC was added, which explains the rapid droplet formation. Their dissolution follows the evolution of the peptide anhydride concentrations very closely, too. The coacervate droplets dissolve as soon as the peptide anhydride concentration falls below the CCC. Before this point is reached, the gradual decrease in turbidity indicates that the droplets also follow the gradual loss in peptide anhydride and therefore the gradual loss of droplet material. In metastable droplets, the decay of the droplets lags the reaction cycle to a certain degree. We can thus conclude that metastable droplets emerge in response to fuel but have a certain degree of stability that does not lead to their immediate decay. Such a delay occurs for peptide **2** with higher-molecular-weight PSS (vide infra). Finally, the droplets based on peptide **4** did not require fuel to form droplets, and the evolution of the turbidity did not change by the addition of fuel (Figure S13).

Role of Polymer Length. Besides the role of the peptide design, the influence of poly(styrenesulfonate) (PSS) chain lengths on the dynamics of the droplets was investigated (Figure 2A). We used turbidimetry at 600 nm for a broad screening of molecular weights ranging from 4.3 kg/mol to 1000 kg/mol. Like the experiments above, we fueled a solution

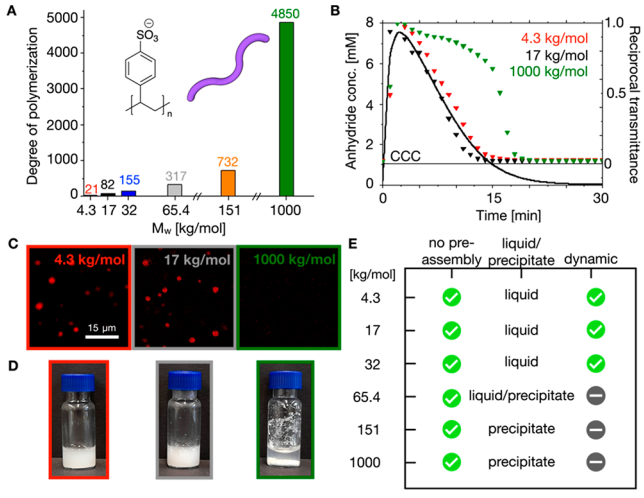

Figure 2. Role of the polymer length on droplet behavior. (A) Different numbers of repeating units (degrees of polymerization) for different poly(styrenesulfonate) polymers used in this study. (B–E) Responses of the system consisting of 25 mM PSS of different chain lengths expressed in monomer units, 16 mM peptide **2**, 50 mM EDC, and 200 mM MES buffer at pH 5.3: (B) Reciprocal transmittance (see Figure 1 and methods for calculation) traces for different poly(styrenesulfonate) lengths (triangles) from plate reader measurements at 600 nm and the evolution of the peptide anhydride concentration (solid line) from the kinetic model. (C) Confocal fluorescence micrographs of coacervate samples in the solution phase for different PSS lengths 4 min into the cycle. The scale bar is 15 μm. (D) Visual turbidity (4.3 kg/mol and 17 kg/mol) of samples during the cycle and precipitation for 1000 kg/mol PSS. (E) Summary of the response for different poly(styrenesulfonate) lengths.

of 16 mM of peptide **2** with 50 mM EDC in 200 mM MES at pH 5.3. We tested the effect of the molecular weight of PSS on the behavior of droplets. It is important to note that in these tests, we are interested in the role of the length of the polymer, not the amount of polymer chains. Thus, in all experiments, the same concentration of PSS was used when expressed in styrenesulfonate monomer units, i.e., 25 mM PSS. In other words, the weight percentage of polymer in solutions was kept the same between experiments.

We found that for PSS with a molecular weight of 4.3, 17, and 32 kg/mol the turbidity of the solution evolved similarly to the experiments described above, from which we conclude that the droplets were dynamic. In contrast, for 65.4 kg/mol or greater, the turbidity decreased at a later point in the cycle. This trend continued with an increasing molecular weight of PSS; e.g., for 1000 kg/mol PSS, the turbidity started to decrease after 15 min. Compared to 17 kg/mol PSS, the turbidity for 1000 kg/mol PSS was also delayed for lower amounts of EDC. The longer cycle lifetimes can be compensated by adding less EDC (Figure S17). We further studied the behavior by confocal microscopy on the shortest (4.3 kg/mol), our standard (17 kg/mol), and the maximum chain length (1000 kg/mol) of PSS (Figure 2C). To our surprise, almost no coacervate droplets of 1000 kg/mol PSS were present in the solution, and the remaining complex coacervates were extremely small compared to the other samples. Instead, the majority of the condensates were found on the surface of the glass slide. The longer PSS chains tended to form smaller complex coacervates that agglomerated and precipitated quickly before they could grow to larger droplets like PSS strands of 4.3 and 17 kg/mol. Those big droplets also settled and wetted the glass surface but kept their droplet shape (Figure S18). We refer to the sediments in samples with 4.3 or 17 kg/mol PSS as liquid-like, because the droplets were able to fuse and wet the surface. In contrast, the precipitates formed by the 1000 kg/mol PSS based system did not show coalescence and maintained rough, irregular shapes. Moreover, they could be observed by the naked eye as transient precipitates (Figure 2D). Bright-field microscopy further revealed that the liquid-to-precipitate transformation occurred for PSS with chain lengths between 65.4 and 151 kg/mol (Figure S18). We correlated the reciprocal transmission to the evolution of the reaction cycle (Figure 2B, Figure S19 C) and found that the evolution of the reciprocal transmittance for samples from 4.3 kg/mol to 32 kg/mol behaved similarly and could be classified as dynamic droplets. In contrast, for 65.4, 151, and 1000 kg/mol, the reciprocal transmittance regained its original values, but that point was several minutes beyond the point where the CCC was reached. The initial values were regained with a delay of 3, 5, and 7 min, respectively (Figure 2B, Figure S19 C). Moreover, the reciprocal transmittance of these samples peaked much beyond the point where the anhydride concentration peaked. We classify those aggregates as metastable by the apparent delay in dissolution compared to the peptide anhydride evolution (Figure 2E).

We explain the different behavior observed for increasing polymer length by a multivalency effect of the poly(styrenesulfonate) chains.[24,25] That means that the greater the polymer chain length, the higher the number of activated product molecules per strand, and thus the more cross-links per polymer chain. This increased number of cross-links leads to delayed disassembly kinetics compared to short polymers. In line with this hypothesis, a study by others has shown that an

https://doi.org/10.1021/jacs.1c01148
J. Am. Chem. Soc. 2021, 143, 4782−4789

increase in polymer length results in increased stability of the coacervate phase toward dissolution induced by salt.[26] We find that a similar mechanism operates because our droplets show similarly increased stability toward salt with increasing polymer chain length (Figure S20). Specifically, when we introduced 250 mM NaCl or more to the system, coacervate droplets from 1000 kg/mol PSS were less affected compared to 17 kg/mol PSS. Moreover, these samples could be refueled even when up to 500 mM NaCl was present, which was not the case for shorter polymer strands. A concentration of 1 M NaCl inhibited complex coacervation completely independent of polymer chain length. Fluorescence recovery after photobleaching (FRAP)-based experiments on droplets formed with 17, 65.4, and 1000 kg/mol PSS further confirmed the different phase regime as it showed a 3-fold decrease in diffusion coefficients of the PSS within the polymer-rich phase from 0.015 $\mu m^2\ s^{-1}$ for 17 kg/mol PSS to 0.005 $\mu m^2\ s^{-1}$ for 1000 kg/mol PSS (Figure S21). Taken together, we showed that our droplets formed by peptide **2** can either be dynamic or metastable depending on the polymer length. This insight offers a valid design tool for controlling the response of complex coacervates to our reaction cycle. Different phase behavior of our active coacervate droplets resulting from different PSS lengths combined with different droplet dynamics resulting from the peptide design will serve as a useful model to mimic the rich phase behavior of membraneless organelles. Besides many fully fluid organelles, examples of more gel-like or even solid phases also exist. The phase behavior of such organelles has a direct implication on their functions.[13]

Role of Polymer Structure. With our increased understanding of regulating the dynamics of the complex coacervate phases, we were interested in controlling their morphology. We modified the nature of the anionic polymer from a simple polyanion to a di- or triblock copolymer by addition of a poly(ethylene glycol) (PEG)-block to our PSS that served as a repulsive block, like the headgroup on a surfactant. Thereby, we anticipated that the PEG-blocks alter the morphology of our complex coacervate droplets.[27,28] We used RAFT polymerization to synthesize two block copolymers, PSS_{77}-*b*-PEG_{105} and PSS_{89}-*b*-PEG_{227}-*b*-PSS_{89} (see Supporting Information and Figure 3A). We tested the behavior of these block copolymers in the presence of peptide **2** under otherwise exactly the same conditions as described above (50 mM EDC added to 16 mM **2**, with 25 mM polymer expressed in monomer units). Compared to the homopolymer, we found lower turbidity levels for the block copolymers, while the lifetime of the turbidity remained the same (Figure 3B). The decreased turbidity is an initial indication that the assemblies are smaller compared to the homopolymer (Figure 3C).

Indeed, cryo-TEM micrographs, 4 min after the addition of EDC, revealed the presence of coacervate core micelles for both block copolymers (Figure 3C). Cryo-TEM on the PSS-PEG-based experiment revealed mainly 100- to 200-nm-long and 30-nm-wide worm-like micelles that were densely packed, while the PSS-PEG-PSS assembled into large spherical assemblies with diameters around 100 nm, likely large compound micelles. DLS analysis showed an intensity distribution with a maximum at 164 nm for PSS-PEG-PSS and a major peak with a maximum of 91 nm for the PSS-PEG complex coacervate micelles (Figure S22). Noteworthy, the block copolymer samples could be refueled, resulting in another round of transient turbidity (Figure S23). We

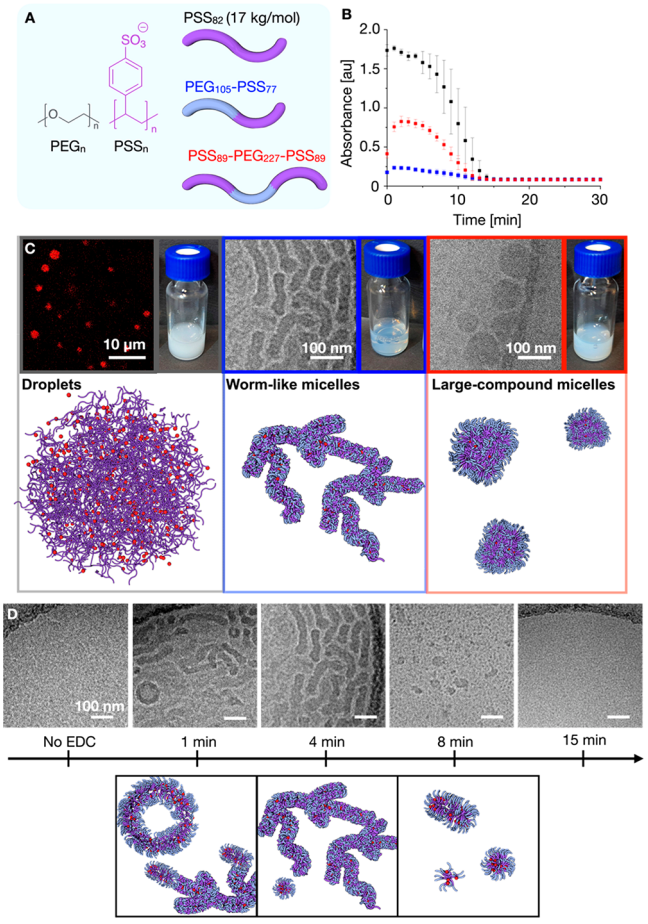

Figure 3. Effect of the polymer nature on the morphology of the phase-separated assembly. (A) Chemical structures of the PSS-PEG block copolymers. (B–D) Analysis of systems with concentrations of 16 mM peptide **2**, 25 mM of homo or block copolymers expressed in styrenesulfonate units and 50 mM EDC in 200 mM MES buffer at pH 5.3: (B) Turbidity traces of PSS homopolymer (17 kg/mol, black), 47.5 kg/mol PSS-PEG-PSS (red), and 21 kg/mol PSS-PEG (blue) from plate reader measurements at 600 nm. (C) Cryo-TEM micrographs of the different coacervate based structures and the visible turbidity of samples 4 min after the addition of EDC. Scale bars are 10 μm (left image) and 100 nm (middle and right image). (D) Different morphologies of PSS_{77}–PEG_{105}-based micelles at different time-points in the reaction cycle. Scale bars are 100 nm.

hypothesize that the PEG block does not partition in the PSS-based complex coacervate core. Thus, the addition of a PEG block resulted in a repulsive block and hindered the unrestricted growth of the PSS block into large droplets. Instead, block copolymer micelles were observed, i.e., worm-like micelles for PSS-PEG and large-compound micelles for PSS-PEG-PSS.

Excited by the drastic change in morphology by the addition of the PEG block, we tested whether the amount of activated peptide in the system affected the phase-separated system's morphology too. We thus further analyzed the PSS_{77}-*b*-PEG_{105} worm-like micelles at different time-points throughout the reaction cycle (Figure 3D). Before the addition of EDC, the cryo-TEM micrograph showed no obvious assemblies. One minute after the fuel was added, a rich mixture of small spherical micelles, long worm-like micelles, and polymersomes was present. After 4 min, only worm-like micelles and spherical assemblies were visible. In the micrograph taken after 8 min,

https://doi.org/10.1021/jacs.1c01148
J. Am. Chem. Soc. 2021, 143, 4782–4789

the decay of the assemblies was clearly evident when only a small fragment of the original micelles remained surrounded by 10 nm globular assemblies. After 15 min, no more obvious assemblies were found.

We explain the morphological transition from polymersomes, to worm-like micelles, to micelles and fragments by a gradual loss of the activated peptide **2**, which is responsible for holding together the PSS-block. The high amount of activated peptide early in the reaction cycle favors the incorporation of more PSS-PEG block copolymers compared to at the later stages. The high density of PEG chains and their repulsion at the micelle corona leads to the elongation of micelles and creates nonspherical shapes like bilayer sheets that form polymersomes and (branched) worm-like micelles, in line with other studies.[29−31] As **2** gradually deactivates, the driving force for the phase separation of the PSS-block decreases, resulting in a gradual loss of block copolymer. The loss of block copolymer results in a decrease in crowding in the corona and less dense packing and thereby a reversion toward micelles that eventually fragment.

Design of Chemically Fueled Coacervate Based Assemblies. Based on the combined findings, we can stipulate pre-emptive design rules for chemically fueled complex coacervate-based assemblies. These rules will hold for designs in which a small molecule transiently increases its number of ionic charges upon chemical activation. Thus, they also apply to the recent designs by Keating[21] and Spruit[32] that use enzymes to activate a precursor by increasing its number of charges. The additional charge increases the affinity for a polymer strand, which can subsequently induce coacervation. When the intention is to form a complex coacervate with a polyanion like our PSS or RNA, the overall charge on the precursor should increase upon chemical activation (+2 in our system). Vice versa, if a polycation like polylysine is to be bound, the overall charge on the precursor should decrease (e.g., by activation via phosphorylation). Whether coacervation will take place depends on the molecular design of the precursor, which, in our case, was gradually altered by the addition of cationic RG-repeats to interact with polyanions. With too little interaction, no coacervation can be expected. On the contrary, if too many groups are added, the precursor itself can also form droplets. Thus, in the molecular design, it is important to find the right balance. In essence, the CCC of the precursor should be higher than the precursor concentration, and, upon activation, that CCC should decrease drastically. Following these design rules, it is reasonable to expect that active droplets can be created using other reaction cycles that change the degree of ionization on their precursor, e.g., the cycle that transiently forms esters at the expense of methylating agents,[33,34] the addition−elimination cycle of dithionite to an aldehyde,[35] and others.[36−38]

On the other hand, the polymer length plays an important role in the design, especially in the dynamics of the emerging droplets. Long polymers result in a loss of the dynamic properties of the droplets due to an increase in the number of cross-links per strand. In other words, if a polymer molecular weight is chosen that is too high, the chemical reactions will become less able to regulate the dynamics of the droplets. Finally, functions can be added to the droplets by adding functional polymers. For example, the droplets are fluorescently labeled when the polymer is fluorescently labeled. Moreover, we show that the morphology of the coacervate can be altered simply by using block copolymers, in which one block has an affinity for the activated peptide, whereas the other does not. In that design, the second block acts as a repelling group like the headgroup on an amphiphile, giving rise to block copolymer amphiphile structures like micelles, worm-like micelles, and polymersomes.

CONCLUSION AND OUTLOOK

We performed a systematic study on the influence of peptide and polymer design on the formation of dynamic and transient droplets. We found that droplet formation could be extremely dynamic when the affinity of the peptide for the polymer was chosen correctly and the polymer length was not too high. Under those conditions, the emergence and decay of droplets evolve with a very high correlation to the chemical reaction cycle that regulates the peptide activation and deactivation. Finally, we found that the polymer's nature can alter the morphology of the complex coacervate based assembly. Our findings allow establishing heuristic design rules for chemically fueled complex coacervate-based assemblies. Such dissipative coacervates will help to mimic the highly dynamic character of membraneless organelles in nature and to elucidate their dynamics and transient properties further.[39]

ASSOCIATED CONTENT

Supporting Information

The Supporting Information is available free of charge at https://pubs.acs.org/doi/10.1021/jacs.1c01148.

Materials and Methods description and additional data (Synthetic protocols and analysis; Sample preparation; Kinetic model; HPLC Procedures and Quenching; CCC determination; Turbidity Measurements; Correlation details; Confocal Fluorescence Microscopy; FRAP procedures; Bright-field microscopy; Cryo-TEM and DLS) (PDF)

AUTHOR INFORMATION

Corresponding Author

Job Boekhoven − *Department of Chemistry and Institute for Advanced Study, Technical University of Munich, 85748 Garching, Germany;* orcid.org/0000-0002-9126-2430; Email: job.boekhoven@tum.de

Authors

Fabian Späth − *Department of Chemistry, Technical University of Munich, 85748 Garching, Germany*

Carsten Donau − *Department of Chemistry, Technical University of Munich, 85748 Garching, Germany*

Alexander M. Bergmann − *Department of Chemistry, Technical University of Munich, 85748 Garching, Germany*

Moritz Kränzlein − *WACKER-Chair of Macromolecular Chemistry, Catalysis Research Center, Technical University of Munich, 85748 Garching, Germany*

Christopher V. Synatschke − *Max Planck Institute for Polymer Research, 55128 Mainz, Germany*

Bernhard Rieger − *WACKER-Chair of Macromolecular Chemistry, Catalysis Research Center, Technical University of Munich, 85748 Garching, Germany;* orcid.org/0000-0002-0023-884X

Complete contact information is available at: https://pubs.acs.org/10.1021/jacs.1c01148

https://doi.org/10.1021/jacs.1c01148
J. Am. Chem. Soc. 2021, 143, 4782−4789

Author Contributions

The manuscript was written through contributions of all authors. All authors have given approval to the final version of the manuscript.

Notes

The authors declare no competing financial interest.

■ ACKNOWLEDGMENTS

This research was conducted within the Max Planck School Matter to Life supported by the German Federal Ministry of Education and Research (BMBF) in collaboration with the Max Planck Society. We thank Christine Rosenauer and Ute Heinz (Max Planck Institute for Polymer Research, Mainz) for aqueous SEC analysis. Cryo-TEM measurements were performed using infrastructure contributed by the Dietz Lab and the TUM EM Core Facility. We acknowledge the technical support provided by Fabian Kohler. F.S., B.R., and J.B. are grateful for funding from the Deutsche Forschungsgemeinschaft via the International Research Training Group ATUMS (IRTG 2022). J.B. is grateful for funding by the European Research Council (ERC starting grant, ActiDrops) under 852187 and funding by the Deutsche Forschungsgemeinschaft (DFG, German Research Foundation) – Project-ID 364653263 – TRR 235 (CRC 235). M.K. thanks the Studienstiftung des deutschen Volkes for their support via their Ph.D. scholarship.

■ REFERENCES

(1) Sing, C. E.; Perry, S. L. Recent progress in the science of complex coacervation. *Soft Matter* **2020**, *16* (12), 2885−2914.
(2) Voets, I. K.; de Keizer, A.; Cohen Stuart, M. A. Complex coacervate core micelles. *Adv. Colloid Interface Sci.* **2009**, *147*−*148*, 300−18.
(3) Sproncken, C. C. M.; Magana, J. R.; Voets, I. K. 100th Anniversary of Macromolecular Science Viewpoint: Attractive Soft Matter: Association Kinetics, Dynamics, and Pathway Complexity in Electrostatically Coassembled Micelles. *ACS Macro Lett.* **2021**, *10*, 167−179.
(4) Zhou, L.; Shi, H.; Li, Z.; He, C. Recent Advances in Complex Coacervation Design from Macromolecular Assemblies and Emerging Applications. *Macromol. Rapid Commun.* **2020**, *41* (21), e2000149.
(5) Schmitt, C.; Turgeon, S. L. Protein/polysaccharide complexes and coacervates in food systems. *Adv. Colloid Interface Sci.* **2011**, *167* (1−2), 63−70.
(6) Blocher, W. C.; Perry, S. L. Complex coacervate-based materials for biomedicine. *Wiley Interdiscip. Rev. Nanomed. Nanobiotechnol.* **2017**, *9* (4), e1442.
(7) Matalanis, A.; Jones, O. G.; McClements, D. J. Structured biopolymer-based delivery systems for encapsulation, protection, and release of lipophilic compounds. *Food Hydrocolloids* **2011**, *25* (8), 1865−1880.
(8) Cabral, H.; Miyata, K.; Osada, K.; Kataoka, K. Block Copolymer Micelles in Nanomedicine Applications. *Chem. Rev.* **2018**, *118* (14), 6844−6892.
(9) De Santis, S.; Diociaiuti, M.; Cametti, C.; Masci, G. Hyaluronic acid and alginate covalent nanogels by template cross-linking in polyion complex micelle nanoreactors. *Carbohydr. Polym.* **2014**, *101*, 96−103.
(10) Kim, H. J.; Yang, B.; Park, T. Y.; Lim, S.; Cha, H. J. Complex coacervates based on recombinant mussel adhesive proteins: their characterization and applications. *Soft Matter* **2017**, *13* (42), 7704−7716.
(11) Dompé, M.; Cedano-Serrano, F. J.; Vahdati, M.; Westerveld, L.; Hourdet, D.; Creton, C.; Gucht, J.; Kodger, T.; Kamperman, M. Underwater Adhesion of Multiresponsive Complex Coacervates. *Adv. Mater. Interfaces* **2020**, *7* (4), 1901785.
(12) Shao, H.; Stewart, R. J. Biomimetic underwater adhesives with environmentally triggered setting mechanisms. *Adv. Mater.* **2010**, *22* (6), 729−33.
(13) Gomes, E.; Shorter, J. The molecular language of membraneless organelles. *J. Biol. Chem.* **2019**, *294* (18), 7115−7127.
(14) Linsenmeier, M.; Kopp, M. R. G.; Grigolato, F.; Emmanoulidis, L.; Liu, D.; Zurcher, D.; Hondele, M.; Weis, K.; Capasso Palmiero, U.; Arosio, P. Dynamics of Synthetic Membraneless Organelles in Microfluidic Droplets. *Angew. Chem., Int. Ed.* **2019**, *58* (41), 14489−14494.
(15) Banani, S. F.; Lee, H. O.; Hyman, A. A.; Rosen, M. K. Biomolecular condensates: organizers of cellular biochemistry. *Nat. Rev. Mol. Cell Biol.* **2017**, *18* (5), 285−298.
(16) Brangwynne, C. P.; Eckmann, C. R.; Courson, D. S.; Rybarska, A.; Hoege, C.; Gharakhani, J.; Julicher, F.; Hyman, A. A. Germline P granules are liquid droplets that localize by controlled dissolution/condensation. *Science* **2009**, *324* (5935), 1729−32.
(17) Rai, A. K.; Chen, J. X.; Selbach, M.; Pelkmans, L. Kinase-controlled phase transition of membraneless organelles in mitosis. *Nature* **2018**, *559* (7713), 211−216.
(18) Mugler, C. F.; Hondele, M.; Heinrich, S.; Sachdev, R.; Vallotton, P.; Koek, A. Y.; Chan, L. Y.; Weis, K. ATPase activity of the DEAD-box protein Dhh1 controls processing body formation. *eLife* **2016**, *5*, e18746.
(19) Weber, C. A.; Zwicker, D.; Julicher, F.; Lee, C. F. Physics of active emulsions. *Rep. Prog. Phys.* **2019**, *82* (6), 064601.
(20) Priftis, D.; Tirrell, M. Phase behaviour and complex coacervation of aqueous polypeptide solutions. *Soft Matter* **2012**, *8* (36), 9396−9405.
(21) Aumiller, W. M., Jr; Keating, C. D. Phosphorylation-mediated RNA/peptide complex coacervation as a model for intracellular liquid organelles. *Nat. Chem.* **2016**, *8* (2), 129−37.
(22) Donau, C.; Späth, F.; Sosson, M.; Kriebisch, B. A. K.; Schnitter, F.; Tena-Solsona, M.; Kang, H. S.; Salibi, E.; Sattler, M.; Mutschler, H.; Boekhoven, J. Active coacervate droplets as a model for membraneless organelles and protocells. *Nat. Commun.* **2020**, *11* (1), 5167.
(23) Schnitter, F.; Boekhoven, J. A Method to Quench Carbodiimide-Fueled Self-Assembly. *ChemSystemsChem.* **2021**, *3* (1), e2000037.
(24) Lu, T.; Spruijt, E. Multiphase Complex Coacervate Droplets. *J. Am. Chem. Soc.* **2020**, *142* (6), 2905−2914.
(25) Priftis, D.; Laugel, N.; Tirrell, M. Thermodynamic characterization of polypeptide complex coacervation. *Langmuir* **2012**, *28* (45), 15947−57.
(26) Chollakup, R.; Beck, J. B.; Dirnberger, K.; Tirrell, M.; Eisenbach, C. D. Polyelectrolyte Molecular Weight and Salt Effects on the Phase Behavior and Coacervation of Aqueous Solutions of Poly(acrylic acid) Sodium Salt and Poly(allylamine) Hydrochloride. *Macromolecules* **2013**, *46* (6), 2376−2390.
(27) Pergushov, D. V.; Muller, A. H.; Schacher, F. H. Micellar interpolyelectrolyte complexes. *Chem. Soc. Rev.* **2012**, *41* (21), 6888−901.
(28) Lemmers, M.; Sprakel, J.; Voets, I. K.; van der Gucht, J.; Cohen Stuart, M. A. Multiresponsive reversible gels based on charge-driven assembly. *Angew. Chem., Int. Ed.* **2010**, *49* (4), 708−11.
(29) Aloi, A.; Guibert, C.; Olijve, L. L. C.; Voets, I. K. Morphological evolution of complex coacervate core micelles revealed by iPAINT microscopy. *Polymer* **2016**, *107*, 450−455.
(30) Takeda, K. M.; Osada, K.; Tockary, T. A.; Dirisala, A.; Chen, Q.; Kataoka, K. Poly(ethylene glycol) Crowding as Critical Factor To Determine pDNA Packaging Scheme into Polyplex Micelles for Enhanced Gene Expression. *Biomacromolecules* **2017**, *18* (1), 36−43.
(31) Osada, K. Development of functional polyplex micelles for systemic gene therapy. *Polym. J.* **2014**, *46* (8), 469−475.
(32) Nakashima, K. K.; Baaij, J. F.; Spruijt, E. Reversible generation of coacervate droplets in an enzymatic network. *Soft Matter* **2018**, *14* (3), 361−367.

https://doi.org/10.1021/jacs.1c01148
J. Am. Chem. Soc. 2021, 143, 4782−4789

(33) Boekhoven, J.; Brizard, A. M.; Kowlgi, K. N.; Koper, G. J.; Eelkema, R.; van Esch, J. H. Dissipative self-assembly of a molecular gelator by using a chemical fuel. *Angew. Chem., Int. Ed.* **2010**, *49* (28), 4825−8.
(34) Boekhoven, J.; Hendriksen, W. E.; Koper, G. J.; Eelkema, R.; van Esch, J. H. Transient assembly of active materials fueled by a chemical reaction. *Science* **2015**, *349* (6252), 1075−9.
(35) Singh, N.; Lainer, B.; Formon, G. J. M.; De Piccoli, S.; Hermans, T. M. Re-programming Hydrogel Properties Using a Fuel-Driven Reaction Cycle. *J. Am. Chem. Soc.* **2020**, *142* (9), 4083−4087.
(36) Grötsch, R. K.; Angi, A.; Mideksa, Y. G.; Wanzke, C.; Tena-Solsona, M.; Feige, M. J.; Rieger, B.; Boekhoven, J. Dissipative Self-Assembly of Photoluminescent Silicon Nanocrystals. *Angew. Chem., Int. Ed.* **2018**, *57* (44), 14608−14612.
(37) Rieß, B.; Grötsch, R. K.; Boekhoven, J. The Design of Dissipative Molecular Assemblies Driven by Chemical Reaction Cycles. *Chem.* **2020**, *6* (3), 552−578.
(38) Wang, G.; Liu, S. Strategies to Construct a Chemical-Fuel-Driven Self-Assembly. *ChemSystemsChem.* **2020**, *2* (4), e1900046.
(39) Yewdall, N. A.; André, A. A. M.; Lu, T.; Spruijt, E. Coacervates as models of membraneless organelles. *Curr. Opin. Colloid Interface Sci.* **2021**, *52*, 101416.

https://doi.org/10.1021/jacs.1c01148
J. Am. Chem. Soc. 2021, 143, 4782−4789